Available online at www.sciencedirect.com
ScienceDirect
Trans. Nonferrous Met. Soc. China 24(2014) 2856−2863
Transactions of Nonferrous Metals Society of China
www.tnmsc.cn

Effect of bias voltage on compositional, mechanical and corrosion property of ZrNbAlN multilayer films by unbalanced magnetron sputtering

Yong-jing SHI[1,2], Fu-sheng PAN[1], Ming-dong BAO[3], Hu-cheng PAN[1], Muhammad RASHAD[1]

1. College of Materials Science and Engineering, Chongqing University, Chongqing 400044, China;
2. Department of Materials Science and Engineering, Chongqing University of Science and Technology, Chongqing 401331, China;
3. Institute of Materials Engineering, Ningbo University of Technology, Ningbo 315016, China

Received 6 August 2013; accepted 13 January 2014

Abstract: Nano-scaled ZrNbAlN films with different negative bias voltages (V_b) were deposited on bronze substrate and Si (100) wafers by a reactive unbalanced magnetron sputtering technique. Composition and structure properties were characterized by X-ray photoelectron spectroscopy and X-ray diffraction. It is found that mole concentrations of Zr and Nb are affected by V_b, which leads to the increase of binding energy of N 1s and Al 2p and decrease of binding energy of Zr $3d_{5/2}$ and Nb $3d_{5/2}$. Surface morphologies evolution controlled by V_b could be observed. Furthermore, X-ray diffraction patterns reveal that these films show a (111) preferred orientation. Moreover, mechanical property and corrosion behavior of ZrNbAlN films were characterized by nanoindentation test and corrosion test, respectively. A maximum value of 21.85 GPa at −70 V occurs in the ZrNbAlN− bronze system, which outperforms uncoated bronze. Corrosion experiments in 0.5 mol/L NaCl and 0.5 mol/L HCl solution show that corrosion potential and corrosion current are dependent on V_b, and better anti-corrosion property could be obtained at −90 V.

Key words: ZrNbAlN multilayer film; magnetron sputtering; composition; corrosion

1 Introduction

Aluminum−bronze alloy as an important structure material was widely used in machinery industry including bearing and parts. In order to enhance surface mechanical property and corrosion resistance of bronze substrates, some surface treatment techniques were developed, such as laser surface modification and thermal spray [1,2]. Moreover, physical vapor deposition (PVD) techniques were also promised and have obtained interesting application, such as cathode arc and magnetron sputtering, which could be used to synthesize films of nitride, oxide and carbide. Transition metal nitride films attracted more scientific interest than carbide and oxide films due to simple synthesis technology and high-speed deposition rate. With the development in magnetron sputtering technique, some novel films materials consisted of multilayer and multiphase, which were synthesized through a combination of multilayer concept and new materials with extremely nanometer-scaled structural ordering [3,4], such as TiN/NbN, Zr−Nb−N and Zr−Al−N [5−9]. Recently, CrTiAlN and TiZrAlN films were synthesized to enhance their physical and chemical stability [10,11]. Several theoretical models describing the effect of hardness enhancement were proposed. It has been proven that the performance of these films was dependent on their microstructure and chemical composition, which could be controlled by basic deposition parameters, such as sputtering power, N_2 flow rate and negative bias voltage (V_b) applied to a substrate during sputtering [12,13]. Especially, the effect of V_b during depositing was reported [14]. In previous research, the properties of ZrNbAlN film controlled by N_2 flow rate were researched [15]. In this work, composition, mechanical and corrosion property of ZrNbAlN with different negative bias voltages synthesized by unbalanced magnetron sputtering were reported.

2 Experimental

Nano-scaled ZrNbAlN multilayer films were synthesized on Al−bronze and silicon (100) substrates

Foundation item: Project (50725413) supported by the National Natural Science Foundation of China; Project (2010BB4290) supported by Natural Science Foundation Project of CQ CSTC, China
Corresponding author: Yong-jing SHI; Tel/Fax: +86-23-65112635; E-mail: yjshi_cqust@163.com
DOI: 10.1016/S1003-6326(14)63418-X

using metallic Zr, Nb and Al targets with 99.95% purity by a reactive DC unbalanced magnetron sputtering system. Sputtering sources were from four element targets arranged at 90° intervals around a stainless steel chamber, and a schematic diagram of film preparation system is shown in Fig. 1. Si (100) substrates were cleaned in acetone using an ultrasonic agitator for 30 min. Before depositing, base pressure was pumped to 7.0×10^{-4} Pa. During film depositing, working pressure was 0.10 Pa, inlet flux rate of Ar gas was fixed at 25 mL/min (standard-state cubic centimeter per minute). Firstly, samples were bombarded by Ar^+ ion for 30 min to eliminate surface adsorption and thin oxide layer. Secondly, the Zr layer and ZrN_x layer were deposited. At last, N_2 gas was put into vacuum chamber to form nitrides, and N_2 flow rate was controlled by a plasma optical emission monitor (OEM) with a feedback control. Sputtering powers of Zr, Al and Nb targets were 8, 7 and 7 mA/cm^2, respectively. Bias voltages of substrate samples were set at −40, −50, −60, −70, −80 and −90 V, respectively. Film thickness was measured using a ball-crater and SEM scale.

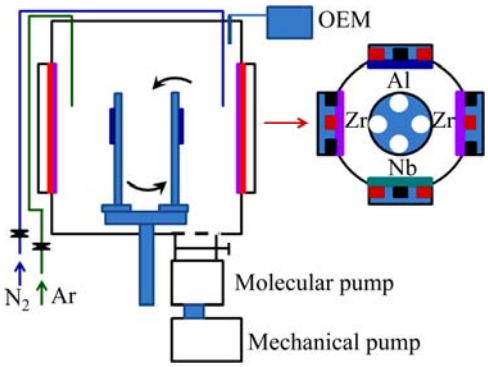

Fig. 1 Schematic diagram of coating preparation system for ZrNbAlN multilayer films

Chemical composition was analyzed by X-ray photoelectron spectroscopy (XPS, ESCALAB250) with Al K_α source (1486.84 eV) radiation and large area XL lens mode, energy step size of 0.1 eV and pass energy of 50 eV. Typical XPS spectra were fitted using Lorentzian−Gaussian function. Binding energy (BE) of surface C 1s spectrum was 285.4 eV for all samples. Surface morphologies were observed with a high resolution field emission scanning electron microscope (FESEM). Cross-sectional morphologies were observed with a high resolution transmission electron microscope (HRTEM, H9000NAR), and fast Fourier transformation spectra (FFT) were obtained from selective area electron diffraction (SAD). Crystallographic microstructure patterns were obtained by grazing incidence X-ray diffraction (GIXRD, Rigaku D/Max 2500), and X-ray source was a Cu K_α radiation at θ=2°. Microhardness and elastic modulus were checked by a Vickers ultra microhardness tester (Fischer scope H100), which were carried out by an indenter at a load of 5 mN. At this load level, indentation depth was much less than one tenth of the film thickness to eliminate the effect of substrate.

Electrochemical corrosion behavior of these films was tested in a solution of 0.5 mol/L NaCl and 0.5 mol/L HCl by an Autolab setup (III+VA663) consisting of three-electrode system. Film samples served as working electrode, and a Pt electrode served as counter electrode kept parallel to working electrode, while a saturated calomel electrode (SCE) served as reference electrode. This reference electrode was kept near surface of working electrode and used to measure the potential of working electrode. Corrosion samples were firstly coated with epoxy resin, leaving only 1.5386 cm^2 surface area exposed, and then coated samples were immersed in corrosion solution for approximately 1 h so that a steady state equilibrium potential, known as open circuit potential (OCP), was obtained. Corrosion experiment was carried out, first cathodically and then anodically, and scan rate and step potential were 0.01 V/s and 0.00213 V, respectively. Scan range was approximately ±0.450 V above OCP to cover Tafel region (±0.060 to ±0.120 V). The polarization curve was recorded simultaneously. Corrosion current density (J_{corr}) and corrosion potential relative to SCE (φ_{corr}) were determined by extrapolating straight-line section of cathodic and anodic Tafel lines of polarization curve.

3 Results and discussion

ZrAlNbN multilayer films were deposited at N_2 flow rate f_N=14 mL/min. Film thickness was 2.0−2.5 μm. To fabricate ZrAlNbN film with multilayer structure, a Zr layer of 50 nm was deposited as the adhesion layer, and then a ZrN_x layer of about 500 nm was deposited, as shown in Fig. 2(a), which shows a TEM cross-sectional morphology of as-deposited film. Figure 2(b) shows interface of film−substrate corresponding to Region 1, yielding a mixing interface layer (several nanometers in thickness) due to ion flux impingement. Figure 2(c) shows interface between ZrN_x and nitride multilayer corresponding to Region 2, indicating the growth direction. Nitride phase clearly presents a periodical modulation structure composed of four layers materials of ZrN, NbN, ZrN, and AlN (Fig. 2(d)). The inset shows micro-area structure and crystallization behavior of nitride multilayer.

Figure 3 shows the relationship between surface morphology evolution and V_b. Granular surface morphologies of ZrNbAlN with different V_b can be seen, and voids in films decrease with the increase in V_b. Surface morphology derived from nucleation and

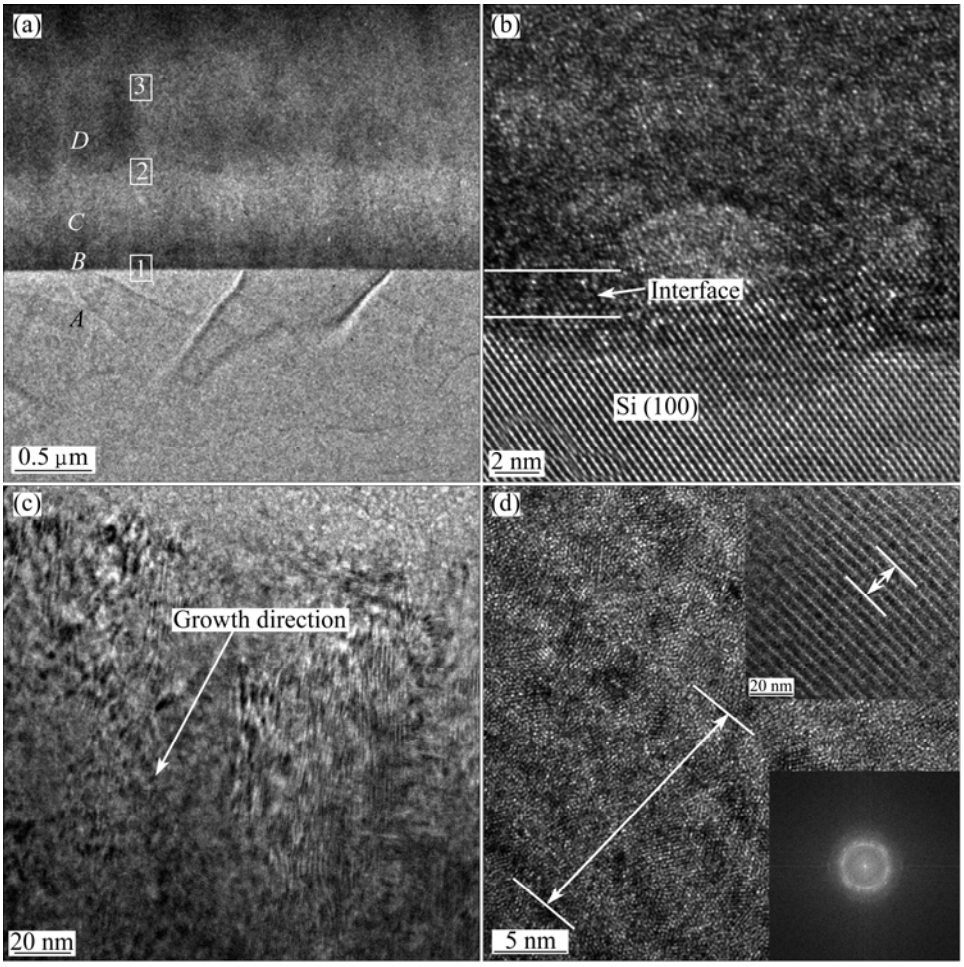

Fig. 2 TEM image of ZrAlNbN films (a) (Regions *A*, *B*, *C*, and *D* represent substrate, adhesion, ZrN_x layer and nitride multilayer, respectively) and HRTEM images of Region 1 (b), Region 2 (c) and Region 3 (d) (Inset is corresponding FFT spectrum)

coalescence of deposition flux during film thickening under low mobility conditions, was dependent on atomic mobility, which could be controlled by impingement energy and ion flux density. Some literatures reported growth model for popular film's deposition was controlled by ion flux [16,17]. Increased V_b caused increase of ion flux to thickening interface, therefore surface roughness decreases. However, surface morphology also could be controlled by thickening rate and temperature, yielding a typical crystallographic microstructure.

Film composition is an important factor affecting film property and structure. Full spectra of these films show that six elements, including O 1s, C 1s, N 1s, Zr 3d, Nb 3d and Al 2p, occur on the surface of these films before etching (Fig. 4). However, the spectra of C 1s and O 1s disappear after being etched. The C 1s derives from an adsorption contaminant from air, while the O 1s derives from residual atmosphere in vacuum chamber during depositing. Mole concentration of O of these films is lower than 3%. Mole ratio of N to metal is about 1:1.1−1:1.2 for all these films. N atomic concentration is seriously affected by V_b, as described in Ref. [17]. Typical XPS spectra were fitted using Lorentzian−Gaussian function, and all the calculated peaks can be assigned to corresponding species (Fig. 5) according to the reference BE from literatures [18−20]. It was found that BE values of N 1s, Zr $3d_{5/2}$, Nb $3d_{5/2}$ and Al 2p at −40 V are 396.78, 179.68, 203.54 and 73.26 eV, respectively, which can be assigned to ZrN (Figs. 5(a, b)), NbN (Figs. 5 (a, c)) and AlN (Figs. 5(a, d)). Moreover, also a few oxynitrides (ZrO_xN_y, NbO_xN_y) and Al_2O_3 formed besides metal Al. These oxynitride species derived from nitrides with dissolved oxygen [21]. Through comparison of several fitting XPS data from ZrNbAlN films with different V_b, it was found that BE is affected by V_b (Figs. 5(e, f)). BE of N 1s and Al 2p increases with the increase in V_b, while BE of Zr $3d_{5/2}$ and Nb $3d_{5/2}$ decreases. Area ratio of nitride increases with the increase in V_b and that of oxynitride according to the calculated data, while that of Al_2O_3 and Al decreases. In order to depict variation of chemical

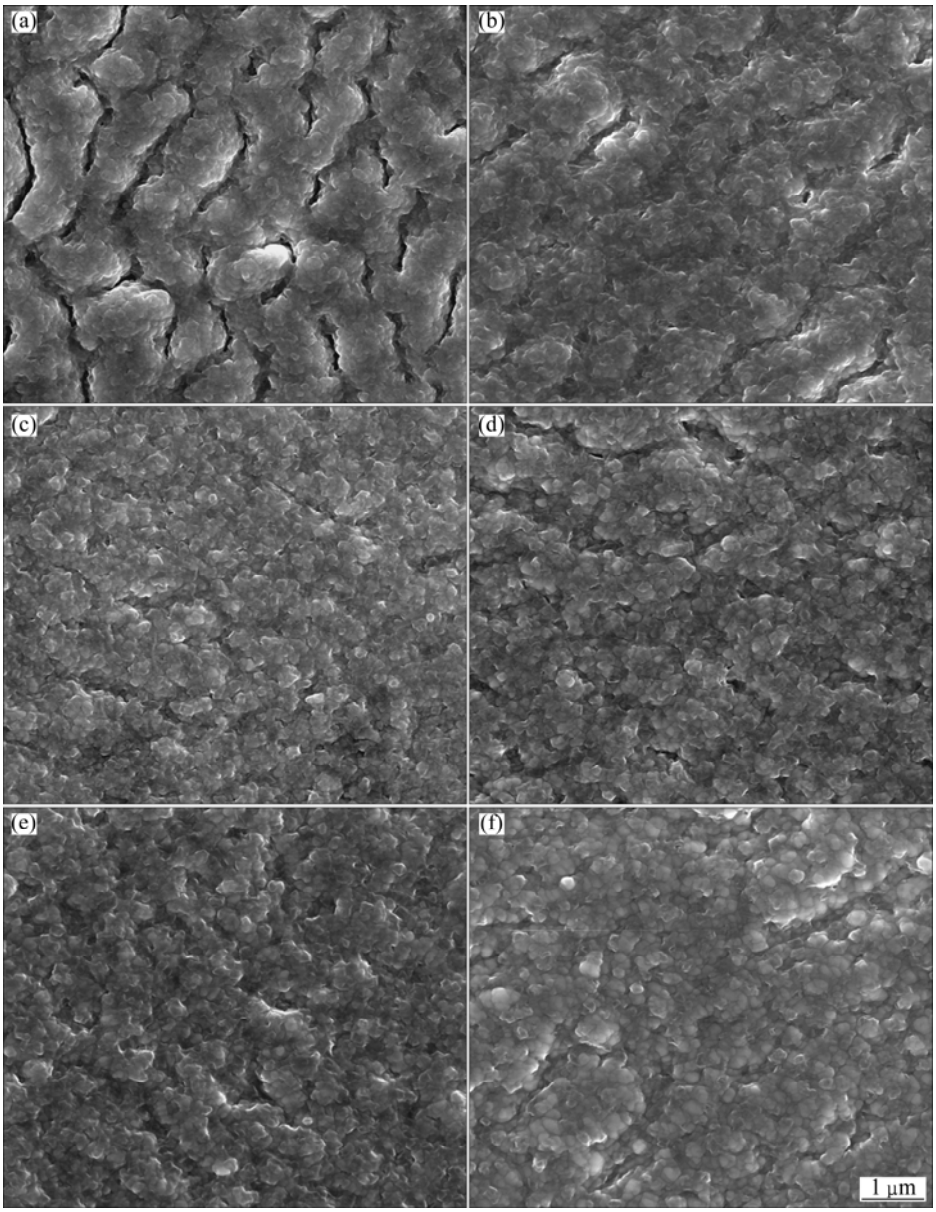

Fig. 3 SEM images of ZrAlNbN films on bronze with different V_b: (a) V_b=−40 V; (b) V_b=−50 V; (c) V_b=−60 V; (d) V_b=−70 V; (e) V_b=−80 V; (f) V_b=−90 V

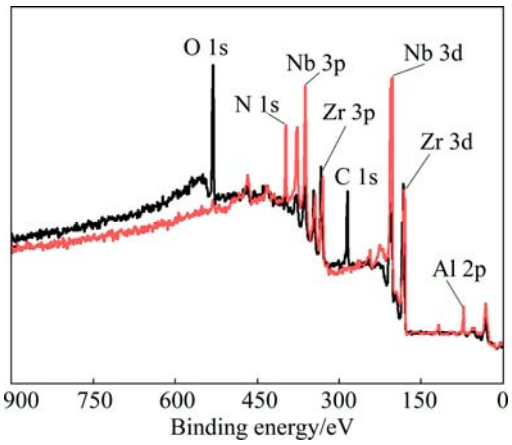

Fig. 4 XPS full spectra of ZrAlNbN film (Black and red curves show XPS spectra before etching and after etching, respectively)

composition at different V_b, relative mole concentration of metal is obtained (Fig. 6). Mole concentration of Zr decreases with the increase in V_b, while mole concentration of Nb increases. However, mole concentration of Al is hardly affected. The phenomenon of relative concentration of metal affected by V_b could be explained by the variation of atomic adsorption rate and different resputtering yields due to ion bombardment during film thickening [22].

Glancing incidence XRD patterns of these films show that there is a relationship between structure of ZrNbAlN films and V_b (Fig. 7). ZrN film presents a crystallographic microstructure of multiphase containing a face-centered cubic (FCC) structure (ZrN, PDF741217) and orthorhombic structure at f_N=12 mL/min and V_b= −40 V (Zr_2N, PDF461204) according to powder

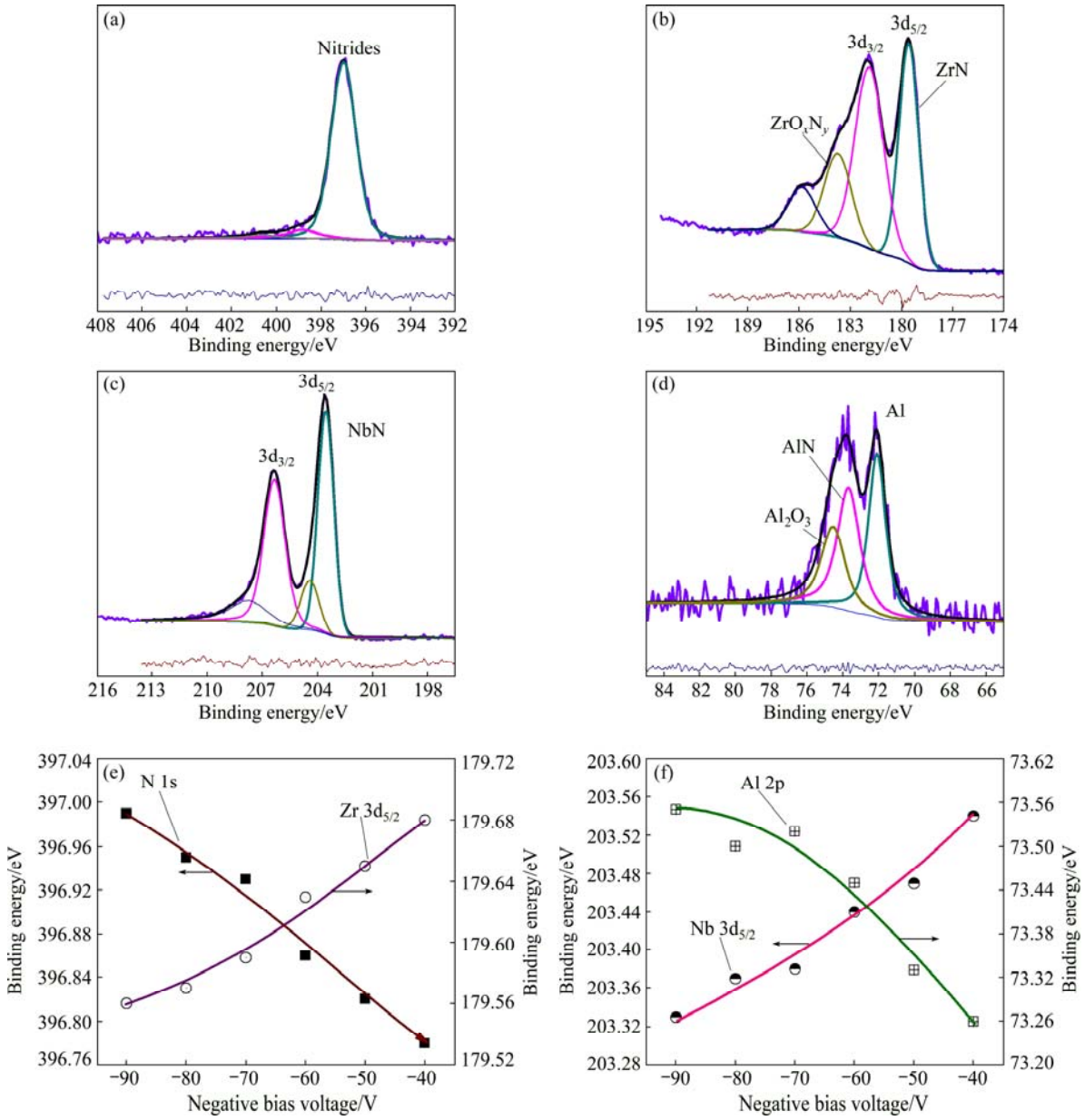

Fig. 5 N 1s spectrum (a), Zr $3d_{5/2}$ spectrum of nitride (b), Nb $3d_{5/2}$ spectrum of nitride (c), Al 2p spectrum of nitride (d) (These XPS spectra were fitted by Lorentzian−Gaussian function, and $\sum\chi 2$ value is lower than 2), BE of N 1s and Zr $3d_{5/2}$ (e) and BE of Nb $3d_{5/2}$ and Al 2p (f)

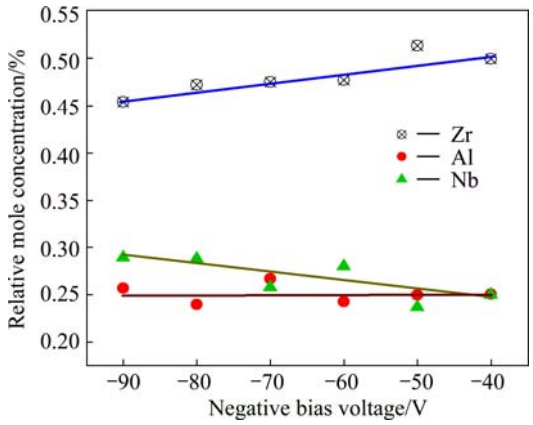

Fig. 6 Relative mole concentration of metal in ZrAlNbN films

diffraction data (JCPDS). ZrNbAlN films show a broadened peak which ranged from 30° to 45° in 2θ value, which could be assigned to FCC structure of (111) out-plane preferred crystallographic orientation according to JCPDS data of ZrN, NbN (PDF741218) and AlN (PDF800010). NbN film showed a phase transition from FCC structure of (200) preferred orientation at V_b=−40 V to mixture phase containing FCC and hexagonal close-packed (HCP) structure at V_b =−80 V [23], and AlN film showed a hexagonal wurtzite-type structure [24]. Obviously, HCP phase could not be observed in ZrNbAlN films. Scherrer's equation revealed that θ value is inversely proportional to grain size.

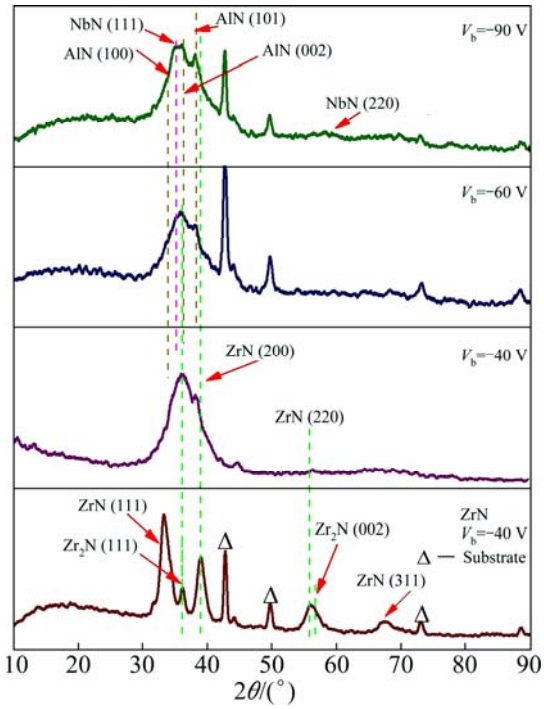

Fig. 7 GIXRD patterns of ZrAlNbN films on bronze (ZrN film was prepared at f_N=12 mL/min)

So, small grain size and low crystallinity could contribute to broadened reflection peak.

Vickers hardness of these films with different V_b on bronze substrates was checked (Fig. 8). Notably, a maximum hardness with 21.85 GPa and elastic modulus with 340 GPa could be obtained at about V_b=−70 V. The inset shows the corresponding bias current (I_b) at different V_b, from which a maximum I_b of 2.14A at V_b=−90 V and a minimum I_b of 1.65 A at V_b=−40 V could be obtained, and I_b shows an exponential increase with the increase in V_b. There is a fact that hardness is dependent on V_b [25,26]. Moreover, Vickers hardness of these films on bronze outperforms that of bronze substrate (3.8 GPa). TUNG et al [27] revealed that the single phase ZrN indicated the maximum micro-hardness at V_b=−80 V. Hardness enhancement can be explained in terms of some following reasons: 1) increased film density [17], 2) higher residual stress [27], 3) strain hardening and high defect density effect.

As a protective film, NaCl and HCl solution on the top of these films in a real work environment may easily cause corrosion degradation, leading to the decrease of service life. Therefore, a conventional potentiodynamic corrosion experiment was carried out in 0.5 mol/L NaCl and HCl solution for ZrNbAlN multilayer films with different V_b. As a reference, potentiodynamic polarization curves of bronze substrate in 0.5 mol/L NaCl and HCl solution are shown in Fig. 9, which shows corrosion potential (φ_{corr}) of −316 mV in 0.5

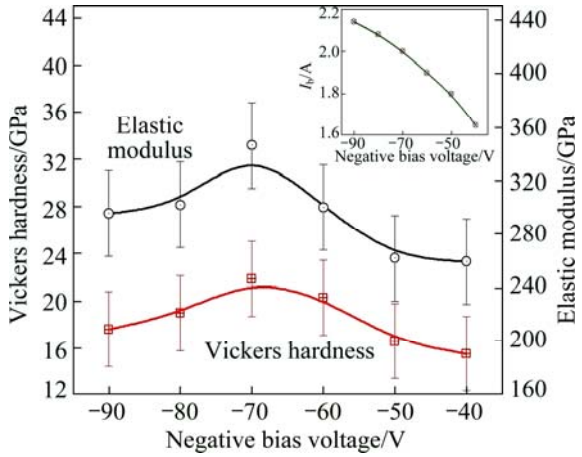

Fig. 8 Vickers hardness and elastic modulus of ZrAlNbN films (Inset shows corresponding V_b−I_b curve)

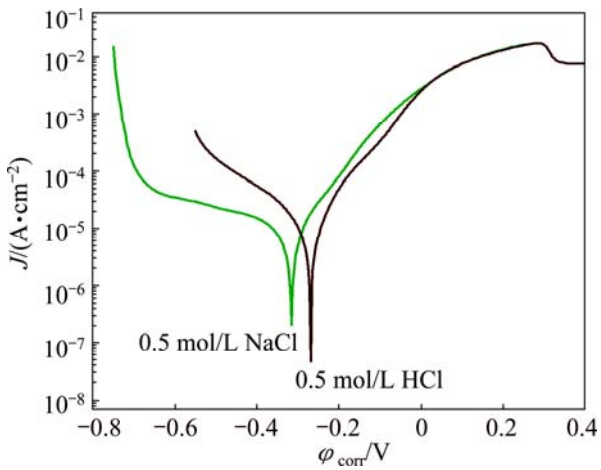

Fig. 9 Polarization curves of bronze substrate in 0.5 mol/L NaCl and 0.5 mol/L HCl solution

mol/L NaCl and φ_{corr} of −269 mV in 0.5 mol/L HCl, yielding a corresponding J_{corr} of 5.523 mA/cm^2 and 4.479 mA/cm^2, respectively. To characterize the bias effect on corrosion behavior, corrosion test of these films was carried out, as shown in Fig. 10. It can be seen that φ_{corr} and J_{corr} in 0.5 mol/L NaCl are higher than those in 0.5 mol/L HCl, leading to φ_{corr} of −200 to −300 mV in 0.5 mol/L NaCl and −230 to −330 mV in 0.5 mol/L HCl. Obviously, it is found that J_{corr} decreases with the increase in V_b, which results in occurrence of the lowest J_{corr} of 0.216 μA/cm^2 in 0.5 mol/L NaCl and 0.622 μA/cm^2 in 0.5 mol/L HCl at V_b=−90 V. φ_{corr} values of ZrN, NbN, AlN were about 210 mV, −420 mV and −566 mV respectively [28−30], which shows that φ_{corr} and J_{corr} firstly depend on material properties. Furthermore, corrosion behavior was seriously affected by V_b, leading to an increase of defect and stress due to the ion flux impingement [31]. So, an excellent anti-corrosion property could be obtained at higher V_b.

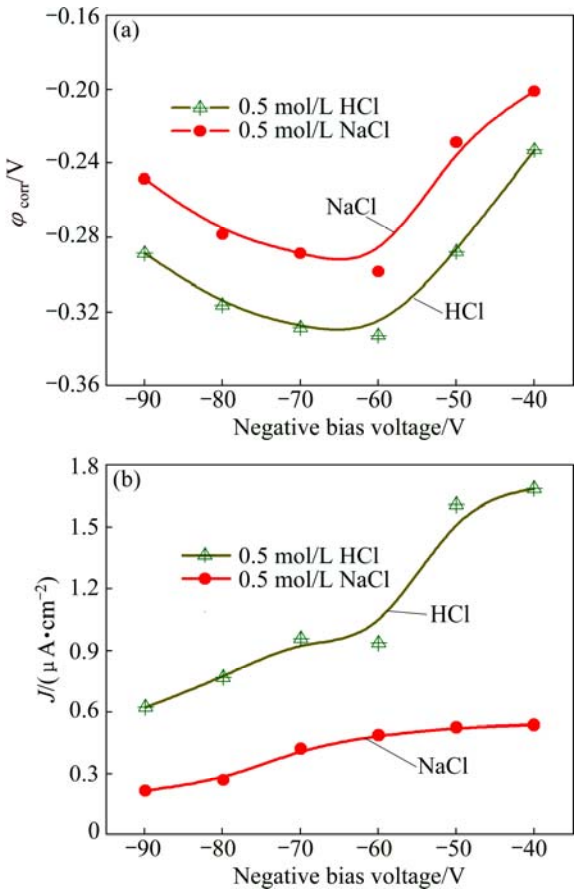

Fig. 10 φ_{corr} (a) and J_{corr} (b) from polarization curve of ZrAlNbN films in 0.5 mol/L HCl and 0.5 mol/L NaCl solutions

4 Conclusions

ZrNbAlN films were successfully deposited on bronze substrate. Composition, mechanical property and corrosion behavior of ZrNbAlN film were characterized. The results reveal that Zr content decreases and Nb content increases with the increase in V_b. XPS analysis shows that BE of N 1s and Al 2p increases with the increase in V_b, while that of Zr $3d_{5/2}$ or Nb $3d_{5/2}$ decreases. There is a notable enhanced mechanical property of surface in the ZrNbAlN film−bronze substrate system, yielding a maximum Vickers hardness of 21.85 GPa and elastic modulus of 340 GPa. Corrosion behavior of ZrNbAlN film was affected by V_b.

References

[1] YILBAS B S, MATTHEWS A, LEYLAND A, KARATAS C, AKHTAR S S, ABDUL A B J. Laser surface modification treatment of aluminum bronze with B4C [J]. Applied Surface Science, 2012, 263: 804−809.

[2] TANG C H, CHENG F T, MAN H C. Laser surface alloying of a marine propeller bronze using aluminium powder: Part I: Microstructural analysis and cavitation erosion study [J]. Surface and Coatings Technology, 2006, 200(8): 2602−2609.

[3] MUSIL J. Hard nanocomposite coatings: Thermal stability, oxidation resistance and toughness [J]. Surface and Coatings Technology, 2012, 207: 50−65.

[4] BRAIC M, BALACEANU M, VLADESCU A, ZOITA C N, BRAIC V. Study of (Zr,Ti)CN, (Zr,Hf)CN and (Zr,Nb)CN films prepared by reactive magnetron sputtering [J]. Thin Solid Films, 2011, 519(12): 4092−4096.

[5] KLOSTERMANN H, FIETZKE F, LABITZKE R, MODES T, ZYWITZKI O. Zr−Nb−N hard coatings deposited by high power pulsed sputtering using different pulse modes [J]. Surface and Coatings Technology, 2009, 204(6−7): 1076−1080.

[6] COOKE K E, BAMBER M, BASSAS J, BOSCARINO D, DERBY B, FIGUERAS A, INKSON B J, RIGATO V, STEER T, TEER D G. Multilayer nitride coatings by closed field unbalanced magnetron sputter ion plating [J]. Surface and Coatings Technology, 2003, 162(2−3): 276−287.

[7] MAKINO Y, MORI M, MIYAKE S, SAITO K, ASAMI K. Characterization of Zr−Al−N films synthesized by a magnetron sputtering method [J]. Surface and Coatings Technology, 2005, 193(1−3): 219−222.

[8] MAKINO Y, SAITO K, MURAKAMI Y, ASAMI K. Phase change of Zr−Al−N and Nb−Al−N films prepared by magnetron sputtering method [J]. Solid State Phenomena, 2007, 127: 195−200.

[9] HOVSEPIAN P E, LEWIS D B, LUO Q, FARINOTTI A. Corrosion resistance of CrN/NbN superlattice coatings grown by various physical vapour deposition techniques [J]. Thin Solid Films, 2005, 488(1−2): 1−8.

[10] ALBERDI A, MARÍN M, DÍAZ B, SÁNCHEZ O, ESCOBAR G R. Wear resistance of titanium−aluminium−chromium−nitride nanocomposite thin films [J]. Vacuum, 2007, 81(11−12): 1453−1456.

[11] KIM Y J, LEE H Y, BYUN T J, HAN J G. Microstructure and mechanical properties of TiZrAlN nanocomposite thin films by CFUBMS [J]. Thin Solid Films, 2008, 516(11): 3651−3655.

[12] CHU K, SHUM P W, SHEN Y G. Substrate bias effects on mechanical and tribological properties of substitutional solid solution (Ti, Al)N films prepared by reactive magnetron sputtering [J]. Materials Science and Engineering B, 2006, 131(1−3): 62−71.

[13] ZHANG S, FU Y, DU H, ZENG X T, LIU Y C. Magnetron sputtering of nanocomposite (Ti,Cr)CN/DLC coatings [J]. Surface and Coatings Technology, 2003, 162(1): 42−48.

[14] PANG X, SHI L, WANG P, ZHANG G, LIU W. Influences of bias voltage on mechanical and tribological properties of Ti−Al−C films synthesized by magnetron sputtering [J]. Surface and Coatings Technology, 2009, 203(10−11): 1537−1543.

[15] SHI Y, PAN F, BAO M, YANG Z, WANG L. Effect of N_2 flow rate on structure and property of $ZrNbAlN_x$ multilayer films deposited by magnetron sputtering [J]. Journal of Alloys and Compounds, 2013, 559: 196−202.

[16] KONG Q, JI L, LI H, LIU X, WANG Y, CHEN J, ZHOU H. Influence of substrate bias voltage on the microstructure and residual stress of CrN films deposited by medium frequency magnetron sputtering [J]. Materials Science and Engineering B, 2011, 176(11): 850−854.

[17] SHI Y J, LONG S Y, YANG S C, PNA F S. Deposition of nano-scaled CrTiAlN multilayer coatings with different negative bias voltage on Mg alloy by unbalanced magnetron sputtering [J]. Vacuum, 2010, 84(7): 962−968.

[18] OLAYA J J, HUERTA L, RODIL S E, ESCAMILLA R. Superconducting niobium nitride films deposited by unbalanced magnetron sputtering [J]. Thin Solid Films, 2008, 516(23): 8768−8773.

[19] JENG J S, CHEN J S. Effects of substrate bias and nitrogen flow ratio on the surface morphology and binding state of reactively sputtered ZrN*x* films before and after annealing [J]. Applied Surface

Science, 2009, 255(19): 8263−8269.

[20] MARCO J F, AGUDELO A C, GANCEDO J R, AUGER M A, SÁNCHEZ O, ALBELLA J M. Corrosion behaviour of AlN and TiAlN coatings on iron [J]. Surface and Interface Analysis, 2006, 38(4): 243−247.

[21] HUANG J H, HU Y Y, YU G P. Structure evolution and mechanical properties of ZrN_xO_y thin film deposited on Si by magnetron sputtering [J]. Surface and Coatings Technology, 2011, 205(21−22): 5093−5102.

[22] WANG Q M, KIM K H. Microstructural control of Cr−Si−N films by a hybrid arc ion plating and magnetron sputtering process [J]. Acta Materialia, 2009, 57(17): 4974−4987.

[23] WEN M, HU C Q, WANG C, AN T, SU Y D, MENG Q N, ZHENG W T. Effects of substrate bias on the preferred orientation, phase transition and mechanical properties for NbN films grown by direct current reactive magnetron sputtering [J]. Journal of Applied Physics, 2008, 104(2): 023527.

[24] FIGUEROA U, SALAS O, OSEGUERA J. Deposition of AlN on Al substrates by reactive magnetron sputtering [J]. Surface and Coatings Technology, 2005, 200(5−6): 1768−1776.

[25] SCHELL N, ANDREASEN K P, BϕTTIGER J, CHEVALLIER J. On the dependence on bias voltage of the structural evolution of magnetron- sputtered nanocrystalline Cu films during thermal annealing [J]. Thin Solid Films, 2005, 476(2): 280−287.

[26] WEBER M, BEWILOGUA K, THOMSEN H, WITTOR R. Influence of different interlayers and bias voltage on the properties of a-C:H and a-C:H:Me coatings prepared by reactive d.c. magnetron sputtering [J]. Surface and Coatings Technology, 2006, 201(3−4): 1576−1582.

[27] TUNG H M, HUANG J H, TSAI D G, AI C, YU G. Hardness and residual stress in nanocrystalline ZrN films: Effect of bias voltage and heat treatment [J]. Materials Science and Engineering A, 2009, 500(1−2): 104−108.

[28] HUANG J H, HSU C Y, CHEN S S, YU G P. Effect of substrate bias on the structure and properties of ion-plated ZrN on Si and stainless steel substrates [J]. Materials Chemistry and Physics, 2003, 77(1): 14−21.

[29] BARSHILIA H C, RAJAM K S. Structure and properties of reactive DC magnetron sputtered TiN/NbN hard superlattices [J]. Surface and Coatings Technology, 2004, 183(2−3): 174−183.

[30] VACANDIO F, MASSIANI Y, EYRAUD M, ROSSI S, FEDRIZZI L. Influence of various nickel under-layers on the corrosion behaviour of AlN films deposited by reactive sputtering [J]. Surface and Coatings Technology, 2001, 137(2−3): 284−292.

[31] LEWIS D B, CREASEY S J, W STEFELD C, EHIASARIAN A P, HOVSEPIAN P E. The role of the growth defects on the corrosion resistance of CrN/NbN superlattice coatings deposited at low temperatures [J]. Thin Solid Films, 2006, 503(1−2): 143−148.

偏压对非平衡磁控溅射 ZrNbAlN 薄膜的成分、力学性能及腐蚀特性的影响

石永敬[1,2]，潘复生[1]，鲍明东[3]，潘虎成[1]，Muhammad RASHAD[1]

1. 重庆大学 材料科学与工程学院，重庆 400044；
2. 重庆科技学院 冶金与材料学院，重庆 401331；
3. 宁波工程学院 材料工程研究所，宁波 315016

摘 要：采用反应非平衡磁控溅射技术在青铜及 Si(100)衬底上沉积不同负偏压(V_b)的纳米 ZrNbAlN 薄膜。薄膜结构及成分采用 X 射线光电子能谱及 X 射线衍射进行表征。结果表明，Zr 和 Nb 的原子浓度受负偏压影响，V_b 导致 N 1s 谱和 Al 2p 谱的结合能增加及 Zr $3d_{5/2}$ 和 Nb $3d_{5/2}$ 谱的结合能降低，薄膜表面形貌的演化受控于 V_b。X 射线衍射谱显示这些薄膜具有(111)择优取向。此外，薄膜的力学特性及腐蚀行为分别通过纳米压痕测试及腐蚀测试表征。当负偏压为−70 V 时，纳米压痕测试显示的最大显微硬度为 21.85 GPa，ZrNbAlN 膜在青铜衬底上的性能远优于未涂层处理的衬底。在 0.5 mol/L NaCl 和 0.5 mol/L HCl 溶液中的腐蚀实验表明，腐蚀势能及腐蚀电流依赖于衬底偏压，在−90 V 时能够获得较高的抗腐蚀特性。

关键词：ZrNbAlN 多层膜；磁控溅射；成分；腐蚀

(Edited by Xiang-qun LI)